Macromolecules

pubs.acs.org/Macromolecules Article

Mechanically Robust Polyvalerolactone Thermosets with Dual Recyclability

Hongyi Gu, Hao Ju, Kun Chen, Chang Sun, Lin Li, Jiayao Chen, Zhen Zhang,* and Peng-Fei Cao*

Cite This: *Macromolecules* 2025, 58, 10037−10047 Read Online

ACCESS | Metrics & More | Article Recommendations | Supporting Information

ABSTRACT: While the incorporation of dynamic covalent bonds (DCBs) in thermosets is widely employed, the materials inevitably downgrade substantially during repetitive physical recycling. Meanwhile, chemical recycling of polymers back to starting monomers often requires significant energy/resource input during the (de/re)polymerization process. To address such a dilemma, we propose a dual-recycling strategy that integrates the advantages of DCBs and chemical recycling by cross-linking chemically recyclable polyesters with DCB-containing cross-linkers. A series of poly(valerolactone) (PVL)-based covalent adaptable networks (CANs) were constructed featuring a functionalized PVL backbone and dynamic boronic-ester-containing cross-linkers to enable simultaneous physical and chemical recyclability. Through fine-tuning the balance between crystallinity and cross-linking density, the CANs exhibited outstanding mechanical properties, including a tensile strength up to 17.7 MPa and an elongation at a break of 1164%. Owing to the dynamic exchange characteristic of boronic esters, the CANs retained nearly identical performance to the original samples after five cycles of physical recycling. Furthermore, the CANs could undergo catalytically assisted chemical recycling with $Sn(Oct)_2$, allowing the recovery of starting monomer. This work provided a valuable approach for the development of dual-recyclable high-performance polymer networks as a potential solution to the current challenges in thermosets recycling.

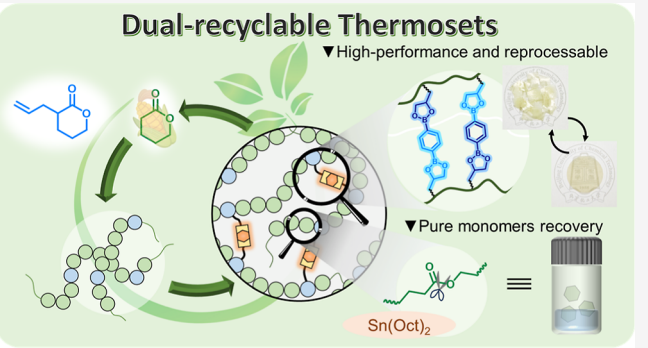

1. INTRODUCTION

Thermosets, composed of chemically cross-linked networks, find widespread applications in aerospace, automotive manufacturing, sports gear, and medical equipment, due to the outstanding mechanical performance as well as superior thermal and chemical resistance.[1−5] However, the structural stability of thermosets renders them nonrecyclable and nonreusable after reaching the end of their functional lifespan.[6−9] Consequently, thermosets are mostly landfilled or incinerated, inevitably leading to soil/groundwater pollution due to the release of microplastics into natural environment and emission of substantial quantities of contaminants.[10−12] With around 65 million tons of thermosets produced annually,[13] few of them undergo recycling or upcycling through various physical, chemical, and biological (de/re)construction strategies. Furthermore, the ever-increasing demand for various polymer thermosets with specifically tailored functionalities, currently synthesized from petroleum-based chemicals, not only exacerbates the impending resource crisis confronting humanity but also poses additional difficulties in their recycling because of the newly designed and typically more complicated structures.[14,15] Such a dilemma highlights the importance of constructing a circular economy mode, which requires the design of novel polymer thermosets that are adaptable and breakable and the development of efficient recycling technologies regardless of the network nature.[16]

Covalent adaptable networks (CANs) with built-in dynamic covalent bonds (DCBs) demonstrate effective reprocessing capabilities through bond exchange/dissociation, positioning them as a potential alternative to traditional thermosets.[17−23] DCBs can be activated by a variety of external stimuli like heat and pressure, facilitating the rearrangements of polymeric network while maintaining its integrity.[24−28] During the past decades, significant progress has been achieved in constructing the commercial polymer-based CANs including polyolefins and polyesters.[29−33] Despite the favorable recyclability, CANs inevitably experience a downgradation in mechanical properties during repetitive physical reprocessing. The molecular chains present in CANs can be broken down by external forces or through oxidative degradation under harsh processing conditions.[34,35] Besides, the side reactions between reactive

Received: April 5, 2025
Revised: July 20, 2025
Accepted: August 26, 2025
Published: September 5, 2025

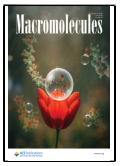

https://doi.org/10.1021/acs.macromol.5c00904
Macromolecules 2025, 58, 10037−10047

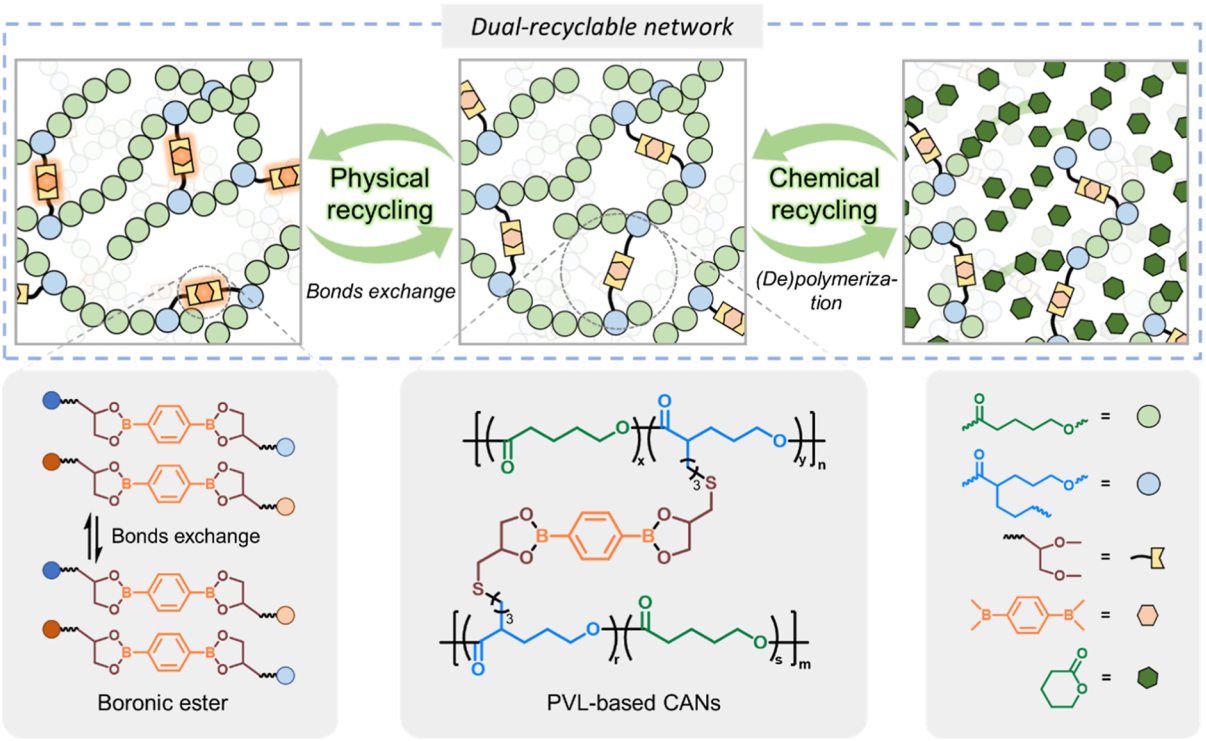

Figure 1. Overview of physical and chemical recycling pathways of the designed CANs. Depiction of boronic ester bonds exchange, the molecular structure of the designed CANs, and the representative signs of chemical structures illustrated the key features of the system.

functional groups, especially under elevated temperature during reprocessing, could permanently cross-link the network and thereby impair its reprocessability. Thus, the physical recycling strategy based on CANs does not fully meet the criteria of circular economy mode, and further recycling measures need to be taken under the circumstance where physical recycling starts to fail. Chemical recycling, on the other hand, refers to the decomposition of polymers containing cleavable bonds into valuable small molecules under specific catalyzed conditions in the presence of light or heat.[36−41] The controlled depolymerization to the corresponding starting monomers enables the subsequent synthesis of fresh materials with comparable properties to their virgin analogues, representing a true circular plastics economy. At present, this approach was mainly applied to thermoplastics such as polyesters and polyurethanes.[42−45] Compared to physical recycling, chemical recycling represents the full utilization of the residual value of discarded polymers yet requires substantial energy consumption due to the (de/re)-polymerization process. Thus, chemical recycling is more suitable as a back-up plan for physical recycling.[46,47]

Considering the disadvantages and advantages of both physical and chemical recycling approaches, we envisioned that a polymeric network composed of dynamic cross-linkers and chemically recyclable repeating units would ensure a reasonable allocation of energy input for (re)processing the materials during/after service while addressing the difficulties in recycling discarded polymers. In 2023, a pioneering work on depolymerizable δ-lactone-based vitrimers was reported by Qi and co-workers.[48] During depolymerization, the weak acetal cross-linkers decompose first to release the linear hydroxyl-terminated polyesters followed by backbiting cyclization reactions from the chain ends that facilitate the monomer recovery. In this case, a weak cross-linker is key that allows the network breakage and subsequent unzipping depolymerization, therefore, the mechanical performance and thermal degradability (decomposition temperature with 5% weight loss, $T_{d,5\%}$ <200 °C) of the material are not ideal, and the selection of cross-linkers is also limited.

To generalize the dual recyclability strategy, we proposed a network architecture integrating depolymerizable polymers with cleavable cross-links, enabling efficient catalytic degradation and high-purity monomer recovery. Such versatility in degradation approaches is fundamentally important for designing polymer networks that simultaneously achieve mechanical robustness and controlled depolymerizability. Guided by such a design principle, we introduced a new type of physically and chemically dual-recyclable polyvalerolactone (PVL)-based CANs with high mechanical performance and superior recyclability. The six-membered lactone, δ-valerolactone (δ-VL), possesses a suitable ring strain that offers fast ring-opening polymerization (ROP) with high efficiency while maintaining the depolymerizability.[49−52] The linear backbone poly(δ-valerolactone-*co*-α-allyl-δ-valerolactone) was synthesized by copolymerizing biosourced δ-VL and α-allyl-δ-valerolactone (α-AVL), with the latter possessing a side allyl group that provides reaction sites (Figure 1). Through reacting with dynamic yet robust boronic ester-based cross-linkers, the mechanical performance was drastically improved.[53] Even after 5 reprocessing cycles, the polymer network still displayed comparable strain and stress to the starting specimen. The boronic ester-based cross-linked networks enabled two distinct recycling pathways owing to their facile transesterification characteristics: direct depolymerization to monomers and deconstruction of the polymer network for enhanced monomer recovery. This depolymerization process remained effective regardless of cross-linker bond strength and could be systematically optimized through pretreatment and catalyst

https://doi.org/10.1021/acs.macromol.5c00904
Macromolecules 2025, 58, 10037−10047

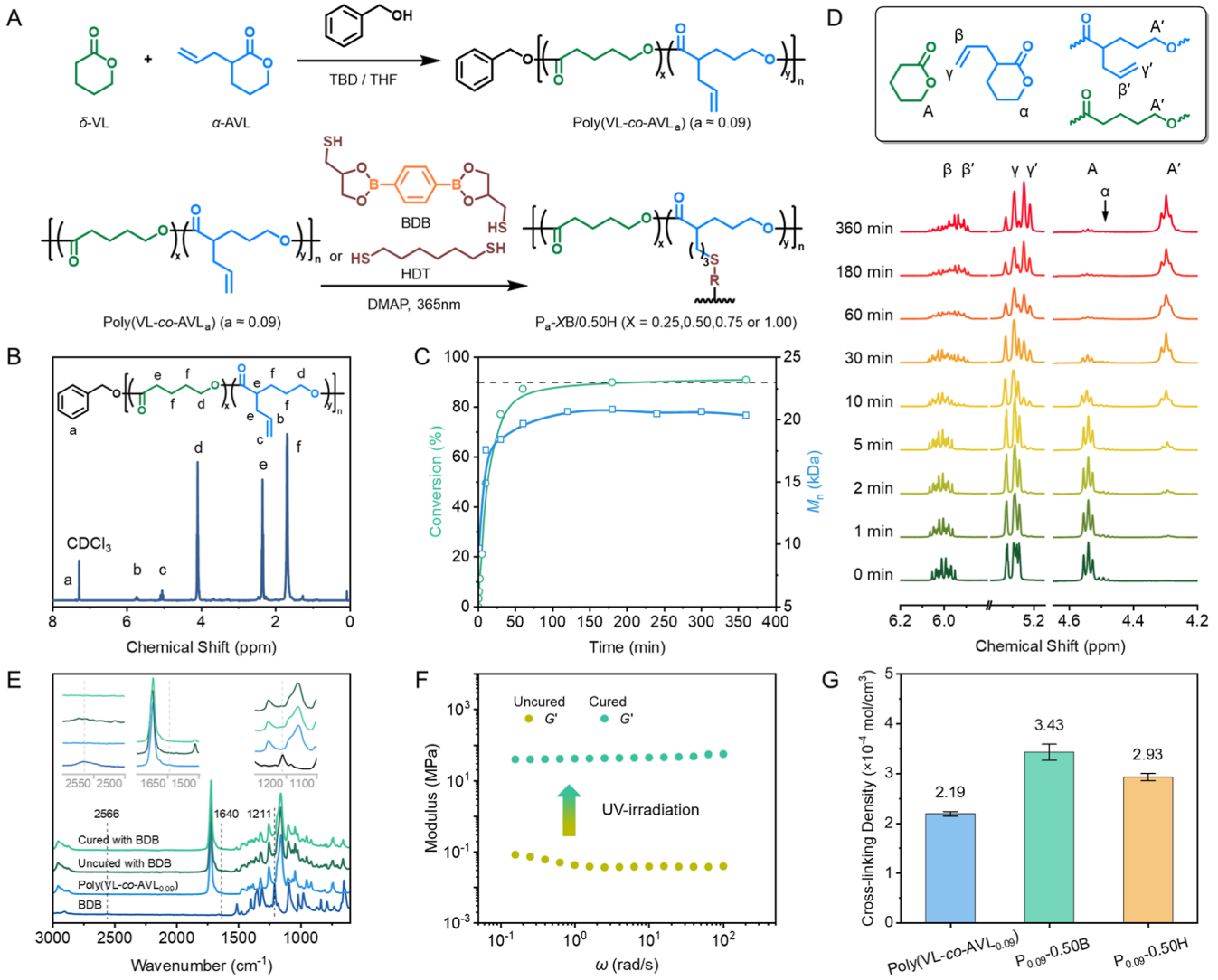

Figure 2. (A) Synthesis of poly(VL-*co*-AVL$_a$) (a ≈0.09) and UV-initiated thiol−ene cross-linking with BDB or HDT. (B) ^{1}H NMR spectra of poly(VL-*co*-AVL$_{0.09}$). (C) Conversion and number-average molecular weight change over time during copolymerization. (D) Time-dependent ^{1}H NMR spectra of copolymerization process (0−360 min). (E) FT-IR spectra of BDB, poly(VL-*co*-AVL$_{0.09}$), and P$_{0.09}$-0.50B before and after UV-irradiation. (F) Storage modulus comparison of uncured and cured CANs at 25 °C. (G) Cross-linking density of poly(VL-*co*-AVL$_{0.09}$), P$_{0.09}$-0.50B, and P$_{0.09}$-0.50H at 25 °C.

selection. The collected colorless liquid was pure monomer, which could be repolymerized with no observable differences with pristine analogue, forming close-loop chemical recycling.

2. RESULTS AND DISCUSSION

2.1. Preparation of Polymer Networks. For the preparation of dual-recyclable CANs, δ-VL and α-AVL with similar ring strain were selected for ROP to synthesize functional polymers with double-bond units randomly inserted for post-functionalization. Subsequently, the functional groups were subjected to thiol−ene "click" chemistry with the dynamic cross-linkers, i.e., (1,4-phenylenebis(1,3,2-dioxaborolane-2,4-diyl))dimethanethiol (BDB) or with the permanent cross-linkers 1,6-hexanedithiol (HDT) to form CANs or permanently cross-linked polymer network (Figure 2A).

To elucidate the reactivity of the selected cyclic monomers δ-VL and α-AVL, a series of experiments were conducted to investigate the thermodynamic polymerizability.[52] At varied reaction temperatures, the five experiments employing 1,5,7-triazabicyclo[4.4.0]dec-5-ene (TBD) as catalyst and benzyl alcohol (BnOH) as initiator were performed with the same initial molar concentration and feeding ratio [α-AVL/δ-VL]/[TBD]/[BnOH] = 500/10/1. At each designated moment, the reaction solution was sampled and quenched with benzoic acid solution. The conversion of δ-VL and α-AVL were calculated through terminal group analysis according to the proton nuclear magnetic resonance (^{1}H NMR) spectra (Figures S6 and S7). Finally, the equilibrium monomer concentration [α-AVL]$_{eq}$ at various temperatures was obtained via conversion plots (Figure S8). The linear relationship between ln[α-AVL]$_{eq}$ and $1/T$, as illustrated in the van't Hoff plot (Figure S9), allows for the calculation of the enthalpy change (ΔH_p) and the entropy change (ΔS_p), which were determined to be −18.2 kJ mol^{-1} and −51.5 J mol^{-1} K^{-1} respectively. According to the equation $T_c = \Delta H_p^{\circ}/\{\Delta S_p^{\circ} + R\ln[M]_0\}$ deduced from Gibbs free energy, ceiling temperature (T_c) of α-AVL was determined as 79.8 °C. Compared to the T_c of δ-VL (262.7 °C at 1.0 M in tetrahydrofuran (THF), Figures S10 and S11), the lower T_c of α-AVL indicates a reduced polymerizability, leading to an undesirable decrease in number-average molecular weight

https://doi.org/10.1021/acs.macromol.5c00904
Macromolecules 2025, 58, 10037−10047

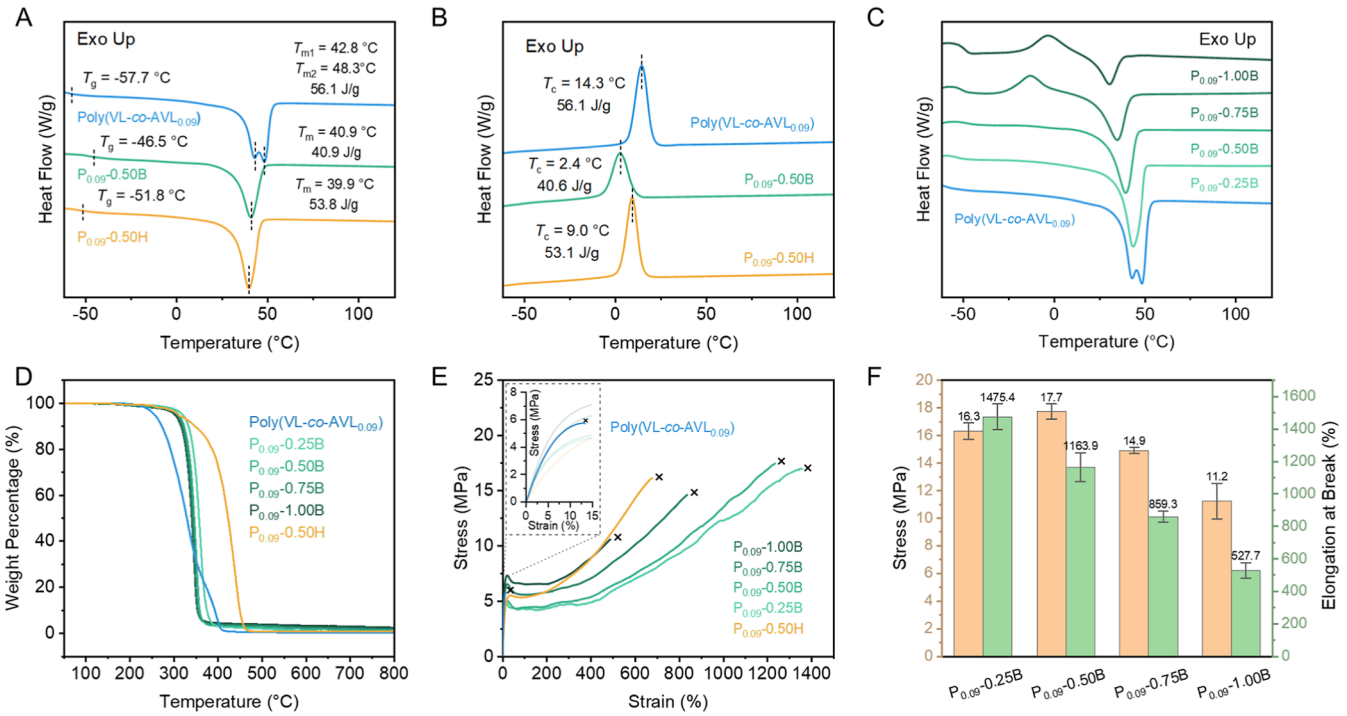

Figure 3. DSC curves of (A) the heating scan and (B) the cooling scan of poly(VL-*co*-AVL$_{0.09}$), P$_{0.09}$-0.50B, and P$_{0.09}$-0.50H. (C) DSC curves of the heating scan of P$_{0.09}$-XBs and poly(VL-*co*-AVL$_{0.09}$). (D) TGA curves of poly(VL-*co*-AVL$_{0.09}$), P$_{0.09}$-XBs and P$_{0.09}$-0.50H. (E) Tensile curves of poly(VL-*co*-AVL$_{0.09}$), P$_{0.09}$-XBs and P$_{0.09}$-0.50H. Inset: tensile curve of poly(VL-*co*-AVL$_{0.09}$) in the 0−15% strain range. (F) Bar chart with SDs showing tensile strength and elongation at break of P$_{0.09}$-XBs.

(M_n) for the poly(VL-*co*-AVL) comparing with PVL (37.1 kDa vs 21.7 kDa).

To optimize the reaction conditions of copolymerization, we explored the ROP by varying the temperatures, solvents, catalysts, and feeding ratios of δ-VL and α-AVL (Table S1). Among the reported organic and metal-complexed catalysts for the ROP of δ-VL, TBD was selected for the investigation of the copolymerization due to its metal-free, highly efficient, and environmentally compatible nature.[54] With THF as solvent, BnOH as initiator, and a fixed α-AVL feeding ratio of 10.0%, lowering the reaction temperature from 25 °C to −40 °C resulted in a notable decrease in the incorporation level of α-AVL from 9.0 to 3.9% as calculated from the ^{1}H NMR spectra (Figure 2B and Table S1, entries 2−4). Given the better copolymerization performance and a suitable M_n at room temperature (∼20 °C), further copolymerization studies were all fixed at ∼20 °C. Varying the amount and ratio of catalyst to initiator effectively tuned the resulting M_n without dramatically affecting the incorporation ratio of α-AVL (Table S1, entries 2, 5, and 6). While increasing the feeding ratios of α-AVL from 10.0% to 50.0%, the incorporation ratio of α-AVL was steadily improved from 9.0% to 44.0% (Table S1, entries 2 and 7−9). Concurrently, the physical form of the products transferred from a white waxy solid to a colorless viscous liquid at room temperature with a marginal variation in the M_n of the products. Replacing the copolymerization solvent from THF to toluene, the M_n gradually decreased, and the dispersity ($Đ$) increased with the increasing incorporation ratio of α-AVL (Table S1, entries 10−12).

During the first hour of polymerization, the α-AVL conversion had not reached an equilibrium value (Figure 2C). After 6 h, the M_n of copolymer slightly increased with incorporation ratio of α-AVL increasing from 6.3 to 9.0%. Prolonging the reaction time from 6 to 12 h led to an increase in dispersity from 1.81 to 2.10, presumably caused by the transesterification after reaching the monomer conversion equilibrium (Table S1, entries 2, 13, and 14). To investigate the kinetics of the copolymerization process, ^{1}H NMR and gel permeation chromatography (GPC) were conducted to monitor the monomer conversion and M_n of the resulting polymers over time. Since the characteristic proton peaks of the two comonomers appeared at a similar position in the ^{1}H NMR spectra after ROP, the monomer conversion used here refers to the total conversion of both monomers (i.e., peak integration: $(A + \alpha)/A'$, Figure 2D). As illustrated in Figure 2C, the copolymerization took place rapidly within the first 50 min, and the M_n of copolymers achieved 21.7 kDa with monomer conversion reaching ∼90% at 200 min, after which the copolymerization did not proceed further. During the copolymerization process, the ^{1}H NMR peaks from the allyl (labeled as $\boldsymbol{\beta}$ and $\boldsymbol{\gamma}$) and δ-CH_2 (labeled as $\boldsymbol{\alpha}$ and **A**) groups of the monomers were gradually shifted from 5.81, 5.09, 4.30, and 4.34 ppm to 5.74, 5.04, 4.06, and 4.06 ppm, respectively (Figure 2D), indicating a smooth copolymerization behavior.

After obtaining the allyl functionalized PVL, we then tried to react with a BDB cross-linker containing dynamic boronic ester bonds (Figure 2A). The "click" reaction between thiol and allyl was initiated by 365 nm UV-irradiation, which is a straightforward, rapid, and practical method for combining modular molecules. We systematically evaluated three different molar ratios of α-AVL incorporation, i.e., 5, 9, and 16%. Decreasing the α-AVL content to 5% resulted in mechanical brittleness, while increasing it to 16% led to poor moldability due to its lower crystallinity and a high proportion of dynamic bonds. Consequently, the polymer network with 9% α-AVL formulation was selected for the following studies due to its

https://doi.org/10.1021/acs.macromol.5c00904
Macromolecules 2025, 58, 10037−10047

optimal mechanical properties. For consistency, the cross-linked polymers were named $P_{0.09}$-XB/H, where 0.09, XB, and XH indicate the incorporation ratio of α-AVL, respectively, and the respective stoichiometric ratios of thiol relative to allyl groups. The successful synthesis of the polymer network was corroborated by Fourier transform infrared (FT-IR) spectra, as shown in Figure 2E. In the case of BDB, the peaks at 2566 cm^{-1} and 1211 cm^{-1} were attributed to the stretching vibrations of −SH and B−O, respectively. For poly(VL-*co*-$AVL_{0.09}$) (the blue trace), the peaks at 1725 cm^{-1} and 1640 cm^{-1} were attributed to the stretching vibrations of >C═O from ester in the main chain and −CH═CH_2 from allyl group in the side chain. Before UV-irradiation, the mixture composed of poly(VL-*co*-$AVL_{0.09}$) and a stoichiometric amount of BDB exhibited characteristic IR peaks from unreacted allyl and thiol groups (dark green trace). After the curing process, the IR signal of the thiol group disappeared, and the characteristic peak corresponding to the disulfide bonds was not detectable (550−450 cm^{-1}, Figure S12), indicating successful cross-linking between thiol and allyl groups. Similarly, the cross-linking reaction between poly(VL-*co*-$AVL_{0.09}$) and HDT demonstrated a comparable change in peak intensity (Figure S13), thereby corroborating the occurrence of the click reaction.

Upon cross-linking, the polymer network typically exhibited a discernible contrast in its storage modulus (G') and loss modulus (G''), as observed in rheological analyses. As illustrated by the room-temperature rheological behavior of the two samples in Figure 2F, in comparison to the samples prior to UV irradiation, the cured samples showed a notable increase in the G' values across a broad frequency ranging from 10^{-1} to 10^2 rad/s. Analysis of cross-linking density using low-field nuclear magnetic resonance revealed a higher cross-linking density of $P_{0.09}$-0.50B and $P_{0.09}$-0.50H relative to poly(VL-*co*-$AVL_{0.09}$) (Table S2), suggesting the successful cross-linking reaction. Herein, different doses of cross-linkers, i.e., 0.25, 0.50, 0.75, and 1.00, were employed to cross-link poly(VL-*co*-$AVL_{0.09}$) under identical reaction conditions, and $P_{0.09}$-0.75B exhibited the highest cross-linking density (Figure S14 and Table S2). This indicated that the network with 1.00 equiv of cross-linker contained a substantial number of ineffective cross-links, whereas maintaining a slight excess of functional groups in the backbones ensured more efficient click reactions. Furthermore, gel fraction analysis demonstrated that $P_{0.09}$-0.50H exhibited a gel content over 99%, confirming the successful construction of a cross-linked polymer network (Figure S15 and Table S3).

2.2. Thermal and Mechanical Characterizations. The differential scanning calorimetry (DSC) was first used to probe the glass transition, melting, and crystallization processes of each sample, as shown in Figure 3A−C. With the high crystallization tendency of δ-VL and α-AVL, the synthesized poly(VL-*co*-$AVL_{0.09}$) exhibited two distinct peaks in the melting process (42.8 and 48.3 °C). As summarized in Table S4, after being cross-linked with BDB or HDT, $P_{0.09}$-0.50B and $P_{0.09}$-0.50H displayed slightly decreased melting temperature (T_m, 40.9 °C vs 39.9 °C), reduced heat of fusion (ΔH_f, 40.9 J/g vs 53.8 J/g), and increased glass transition temperature (T_g, −46.5 °C vs −51.8 °C) due to the restricted polymer chain mobility. Despite having the same cross-linking molar ratio, $P_{0.09}$-0.50B displayed a substantially smaller ΔH_f value relative to that of $P_{0.09}$-0.50H (40.9 J/g vs 53.8 J/g), which was likely caused by the higher structural rigidity of the BDB unit that more effectively disrupted the packaging capability of polymer chains. During the cooling process, the polymers underwent crystallization in a manner consistent with the heating results, where poly(VL-*co*-$AVL_{0.09}$) had the highest crystallization enthalpy (ΔH_c) and crystallization temperature while $P_{0.09}$-0.50B had the lowest ΔH_c. To further investigate the influence of cross-linking densities on the crystallization process, the DSC curves of $P_{0.09}$-XBs, with various amounts of BDB cross-linker, were measured under the same conditions with a heating ramp of 10 °C/min. $P_{0.09}$-0.25B, with a slightly cross-linked network, displayed a thermal transition behavior similar to that of the parent copolymer. Through increasing the molar ratio of BDB to 0.75 and 1.00 equiv, the obtained polymer networks, $P_{0.09}$-1.00B and $P_{0.09}$-0.75B, started to display a crystallization peak on the second heating scan (Figure 3C), indicating a drastically reduced crystallization rate with enhanced cross-linking density. Consistently, the CANs exhibited a gradually decreased crystallization temperature from 14.3 to −15.2 °C when increasing the molar ratios of BDB from 0 to 0.75 (Figure S16). Compared with $P_{0.09}$-1.00B and $P_{0.09}$-0.75B, $P_{0.09}$-0.50B possessed a delicate balance between cross-linking and crystallization. As illustrated by the thermogravimetric analysis (TGA) (Figure 3D and Table S5), poly(VL-*co*-$AVL_{0.09}$) displayed a $T_{d,5\%}$ of 285 °C. After cross-linking, the $P_{0.09}$-XBs and $P_{0.09}$-XH displayed substantially improved thermal stability with $T_{d,5\%}$ exceeding 300 °C, attributed to the improved structural stability. However, when increasing the amount of cross-linkers from $P_{0.09}$-0.25B to $P_{0.09}$-1.00B, $T_{d,5\%}$ gradually decreased from 318.2 to 308.3 °C. Fundamentally, we attributed this phenomenon to the release of boron-containing small molecules that possess Lewis acidity at elevated temperatures. The released species could activate the breakage of ester bonds, which not only depressed the $T_{d,5\%}$ of $P_{0.09}$-0.50B relative to $P_{0.09}$-0.50H but also reduced the thermal stability of dynamically cross-linked covalent networks with higher cross-linker contents.[55]

To investigate the mechanical properties of synthesized polymers, tensile tests were performed with stress−strain curves displayed in Figure 3E, and mechanical parameters, including Young's modulus (E), yield strength (σ_Y), tensile strength (σ_B), and elongation at break (ε_B), were summarized in Figure 3F and Table S6. Due to the high crystallinity, poly(VL-*co*-$AVL_{0.09}$) displayed high brittleness, resulting in a high modulus (E = 92.9 ± 7.8 MPa) and a low extensibility (ε_B = 11.6 ± 1.8%), as shown in Figure S17. Upon cross-linking, the resulting polymers displayed enhanced extensibility and tensile strength, as evidenced by the pronounced plastic deformation characteristics in the tensile curves. At the start of elastic deformation, $P_{0.09}$-XBs showed a similar modulus with poly(VL-*co*-$AVL_{0.09}$) due to their comparable degree of crystallinity. With the continuous stretching, the deformation of splines transformed from elastic to plastic at an elongation value of ∼20% with the stress reaching the yield point. At the yield point, $P_{0.09}$-1.00B and $P_{0.09}$-0.75B displayed a higher strength than $P_{0.09}$-0.50B and $P_{0.09}$-0.25B due to a denser network. After that, the splines underwent strain softening characterized by decreased stress and cold-drawing process where the strain increased while the stress remained constant. Following the cold-drawing phase, the crystallized polymers underwent strain hardening, leading to constant increased stress. Overall, cross-linking enhanced the mechanical properties of polymers in which $P_{0.09}$-0.50B had the highest tensile strength (σ_B = 17.7 ± 0.6 MPa), and $P_{0.09}$-0.25B had the

https://doi.org/10.1021/acs.macromol.5c00904
Macromolecules 2025, 58, 10037−10047

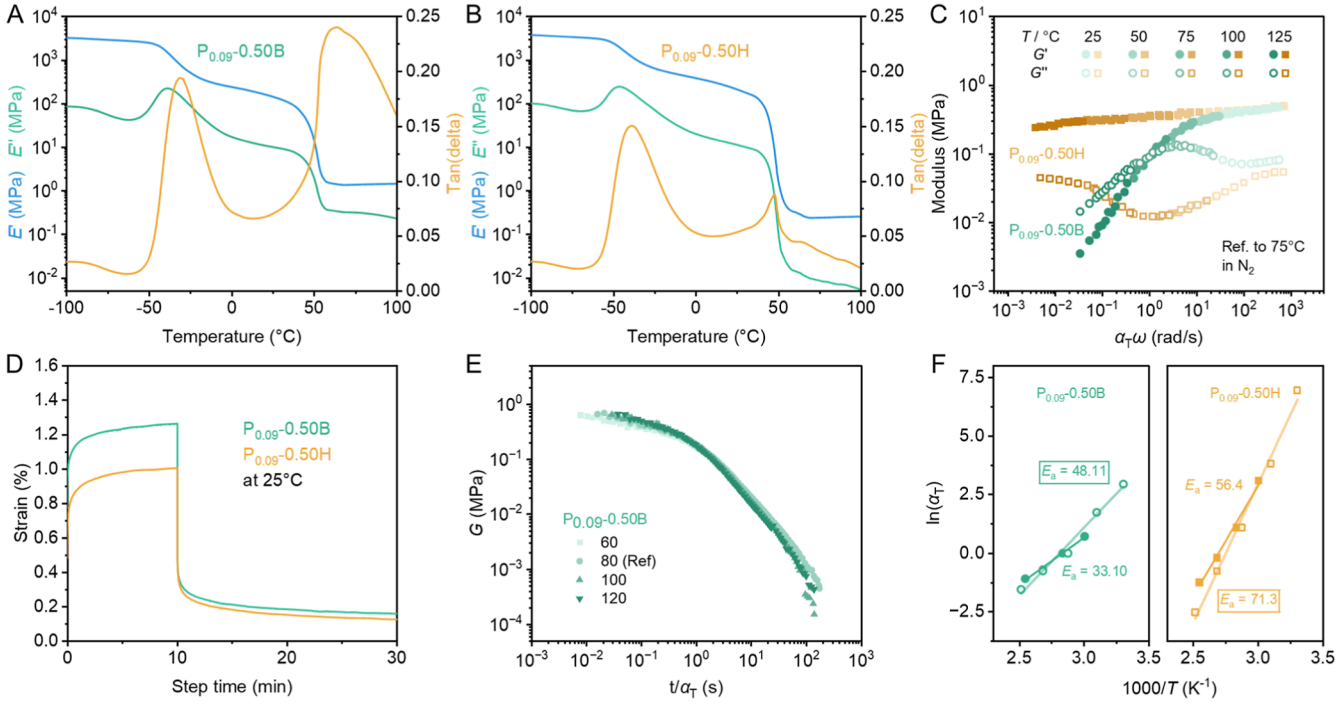

Figure 4. DMA curves of (A) $P_{0.09}$-0.50B and (B) $P_{0.09}$-0.50H within the range of −100 to 100 °C. (C) Rheological master curves of $P_{0.09}$-0.50B and $P_{0.09}$-0.50H from 25 to 125 °C with a reference temperature at 75 °C in N_2. (D) Creep curves of $P_{0.09}$-0.50B and $P_{0.09}$-0.50H at 25 °C. (E) Stress relaxation curves of $P_{0.09}$-0.50B at varying temperatures. (F) For $P_{0.09}$-0.50B and $P_{0.09}$-0.50H, linear regression analyses conducted between the natural logarithms of the shift factors ($\ln(\alpha_T)$) of stress relaxation (solid) and master curves (hollow), and the reciprocal of the temperature ($1/T$), unit of E_a: kJ/mol.

highest extensibility (ε_B = 1475 ± 79%). It can be observed that the cross-linking density of these CANs positively correlates with yield strength and negatively with elongation at break, indicating an effective way to tune the mechanical properties of CANs. Compared to $P_{0.09}$-0.50H with ε_B = ∼717% and σ_Y = ∼5.4 MPa, $P_{0.09}$-0.50B displayed a much higher extensibility of 1164% and similar σ_Y = ∼5.3 MPa (Table S6), due to the dynamic nature of BDB cross-linker that could effectively dissipate the external energy via structural rearrangement during drawing yet maintaining the constant cross-linking density. The mechanical performance of the current PVL thermosets is comparable or superior to state-of-the-art recyclable thermosets, such as polycarbonates, polyureas, poly(ketoenamine), and polyschiff (Figure S18 and Table S7).

2.3. Dynamic Properties Analysis. Dynamic mechanical analysis (DMA) was implemented to analyze the temperature-dependent dynamic behavior of poly(VL-*co*-$AVL_{0.09}$), $P_{0.09}$-XBs, and $P_{0.09}$-0.50H. As shown in Figure 4A,B, a transition peak in tan δ, derived from segmental relaxation, was observed in the temperature range from −50 to −25 °C in each sample. Such a peak in the tan δ curve at glass transition temperature was also observed in the temperature sweep rheology curve for poly(VL-*co*-$AVL_{0.09}$) from −100 to 100 °C (Figure S20) followed by a stable shear modulus subsequent. In Figure 4A,B, the storage modulus (E') and loss modulus (E'') of polymer networks underwent rubbery plateaus with a small dip as the temperature rose above T_g, followed by a distinct decrease (secondary peaks of tan δ) that could be attributed to the melting of crystalline domains. The $P_{0.09}$-0.50B displayed a more pronounced secondary peak of tan δ than $P_{0.09}$-0.50H possibly due to the additional energy loss stemming from dynamic bonds exchange. As the temperature elevated above the melting point (T_m) of the linear backbone, the modulus of poly(VL-*co*-$AVL_{0.09}$) declined until G'' surpassed G', reaching a flow state, while the $P_{0.09}$-0.50B and $P_{0.09}$-0.50H maintained a stable modulus due to the cross-linked network. The melted crystallization in CANs resulted in a significant decrease in G', promoted network rearrangement, diminished the restriction imposed on the dissociation, exchange, and association of boronic ester bonds.

To further investigate the dynamics upon relaxation, rheology master curves of $P_{0.09}$-0.50B and $P_{0.09}$-0.50H were constructed using time−temperature superposition (TTS) as illustrated in Figure 4C. At high frequency, the CAN, i.e., $P_{0.09}$-0.50B, exhibited a relatively high modulus with $G' > G''$, indicating typical solid behavior. As the frequency decreased, G'' and G' of CANs decreased continuously until an intersection at 75 °C, while no such modulus crossover could be seen in the case of the permanent cross-linked network ($P_{0.09}$-0.50H), indicating the key role of dynamic boronic ester bonds in the terminal relaxation behavior in CANs.

We further studied the typical creep behaviors of $P_{0.09}$-0.50B and $P_{0.09}$-0.50H, as illustrated in Figure 4D. Following the application of 1 MPa stress to each sample for a period of 10 min at room temperature, the strain of $P_{0.09}$-0.50B was significantly higher than that of $P_{0.09}$-0.50H, while both systems reverted to a similar strain after the removal of external force. This could be explained by the fact that the aliphatic chains employed as permanent cross-linkers provided reliable creep resistance through limiting chain mobility within the networks under stress, while the dynamic cross-links within CANs can undergo topological rearrangement under external stress. Such dynamic behavior could release part of the energy and speed

https://doi.org/10.1021/acs.macromol.5c00904
Macromolecules 2025, 58, 10037−10047

Table 1. Activation Energies (E_a) of $P_{0.09}$-XBs and $P_{0.09}$-0.50H Calculated From Stress Relaxation and Master Curve Shift Factors Methods

sample	$P_{0.09}$-0.25B	$P_{0.09}$-0.50B	$P_{0.09}$-0.75B	$P_{0.09}$-1.00B	$P_{0.09}$-0.50H
E_a (kJ/mol)[a]	34.6	33.1	19.1	18.4	56.4
E_a (kJ/mol)[b]		48.1			71.3

[a]Stress relaxation method. [b]Master curve shift factors method.

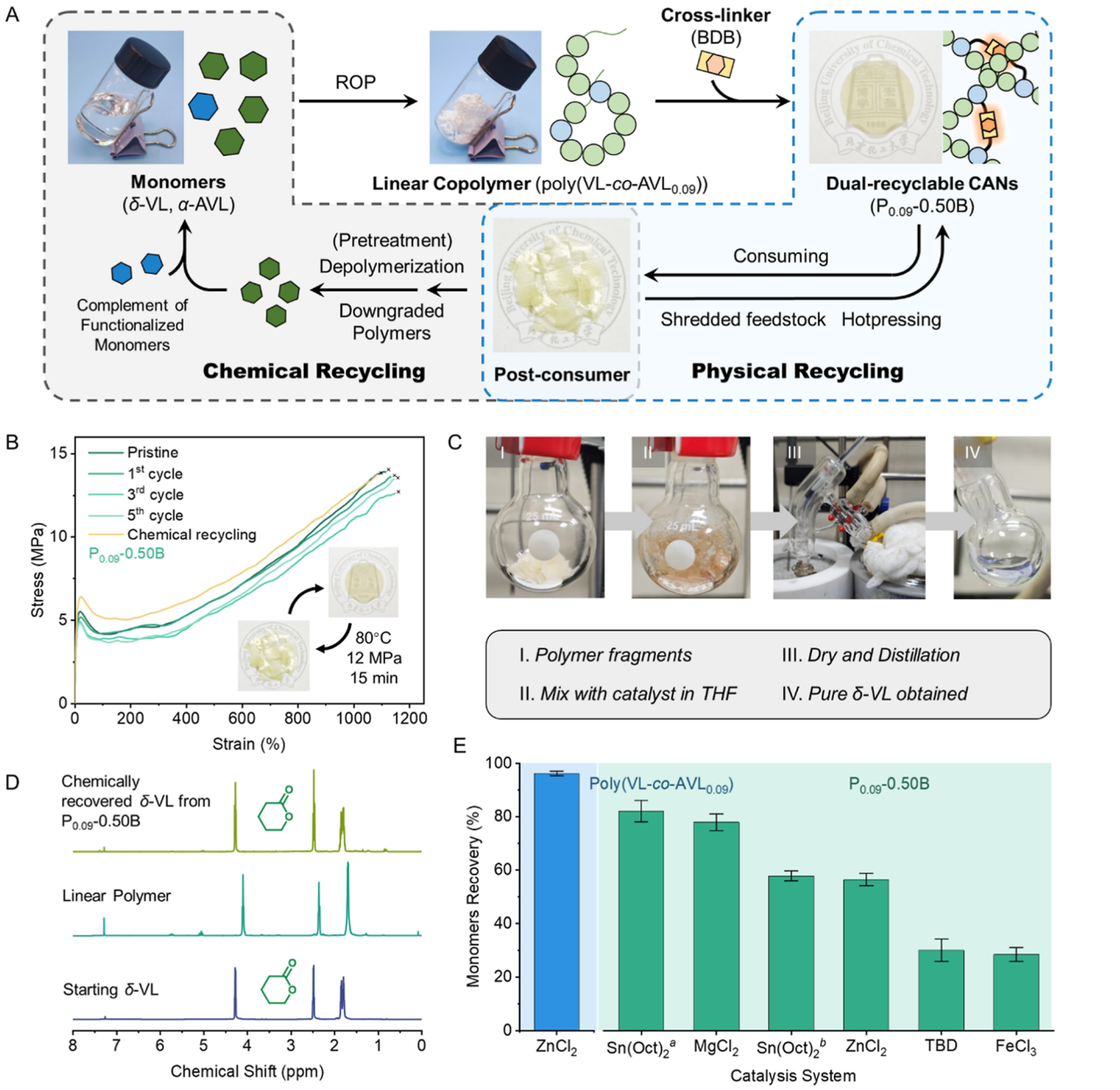

Figure 5. (A) Full life cycle of dual-recyclable CANs: from copolymerization, cross-linking, consuming to dual-recycling (mechanical reprocessing and chemical depolymerization), and repolymerization from chemically recovered monomers. (B) Tensile curves of $P_{0.09}$-0.50B in its pristine state, after 1, 3, and 5 cycles of thermal recycling process, and chemical recycling process. (C) Typical procedures of chemical recycling. (D) ^{1}H NMR (25 °C, in $CDCl_3$) comparison of starting δ-VL, poly(VL-*co*-$AVL_{0.09}$), and chemically recovered δ-VL from CANs. (E) Monomer recovery efficiency of various depolymerization catalysts ([a]boronic ester transesterification pretreatment, [b]direct depolymerization).

up the chain mobility, resulting in a reduction in creep resistance.

The stress relaxation behaviors of $P_{0.09}$-XBs and $P_{0.09}$-0.50H were examined at varying temperatures (Figures 4E and S22–S26), holding a 1% shear strain within the linear viscoelastic region of CANs and $P_{0.09}$-0.50H (Figure S21). Both $P_{0.09}$-0.50B and $P_{0.09}$-0.50H exhibited stress relaxation behaviors at elevated temperatures. From the perspective of chain dynamics, despite both systems possessing cross-linked networks, significant crystallization of polymer chains occurred. The melting behavior of crystal domains above T_m subsequently intensified the chain mobility and led to abrupt

https://doi.org/10.1021/acs.macromol.5c00904
Macromolecules 2025, 58, 10037−10047

stress relaxation. Although the dynamic exchange of the boronic ester in $P_{0.09}$-0.50B possessed dynamic characteristics that facilitate topological rearrangement, its segmental mobility remained constrained by associative exchanges. Conversely, the permanent cross-links in $P_{0.09}$-0.50H restricted sustained stress relaxation at high temperatures. To account for the hierarchical relaxation modes in dynamically adaptable networks, we employed a stress relaxation shift factor method for calculating the activation energy (E_a) of DCBs.[56,57] Similarly, the TTS method was applied to stress relaxation curves, yielding horizontal shift factors at multiple temperatures. According to the Arrhenius equation, there is a linear relationship between $1/T$ and $\ln(\alpha_T)$. The horizontal shift factors of stress relaxation and rheological master curves against $1/T$ were plotted individually to calculate the E_a values of CANs (Figures 4F, S26 and Table 1). It was obvious that the E_a decreased with increased cross-linking density, attributed to the fact that the CANs with higher dynamic cross-linking density had increased chances for dynamic bonds to find their partners during exchange processing.[58,59] The permanently cross-linked $P_{0.09}$-0.50H exhibited the highest E_a due to its significantly restricted chain mobility and absence of sticky bonds for energy dissipation.

2.4. Dual-Recycling Behaviors of CANs. Traditionally, CANs can be repaired, healed, or recycled through reprocessing under specific conditions, and the cross-linking density of associative CANs is claimed to be relatively constant during reprocessing.[60,61] Herein, CANs containing dynamic boronic ester bonds were designed for the release of internal stress and efficient rearrangement of the network topology. Especially, utilization of cleavable polymer chains as CAN backbones endowed them with chemical recyclability, thus forming dual-recyclable CANs. The full life cycle of CANs was illustrated in Figure 5A, commencing with two monomers and progressing via ROP to form functionalized polymer chains. Subsequently, a "click" reaction with dynamic-bond-containing cross-linkers resulted in the formation of dual-recyclable polymer networks. The CANs could be physically recycled by thermal reprocessing with retained high cross-linking densities over 5 cycles (Figures 5B, and S28−S30). Thereafter, the CANs could be catalytically depolymerized to recover the initial monomer through vacuum distillation, which could be reused for the synthesis of a virgin-quality linear copolymer and corresponding networks.

To address the downgradation after several physical recycling processes and enable dual recycling capability, we put forward a strategy of introducing degradable backbones into CANs based on previous research on ROP and ring-closing depolymerization. The ability of magnesium chloride ($MgCl_2$), ferric chloride ($FeCl_3$), zinc chloride ($ZnCl_2$), Sn(II)$_2$-ethylhexanoate ($Sn(Oct)_2$), TBD, and tri[*N*,*N*-bis(trimethylsilyl)amide]lanthanum(III) ($La[N(SiMe_3)_2]_3$) to degrade aliphatic polyesters was investigated as a potential means of facilitating network degradation. The TGA thermograms demonstrated that all selected catalysts significantly reduced the $T_{d,5\%}$ of polymers (Figure S31). Additionally, to investigate the role of pretreatment in its degradation process, we attempted to disrupt the network structure of CANs through acidolysis, alkaline hydrolysis, and transesterification prior to depolymerization. As illustrated in Table S9, $ZnCl_2$ was initially selected as the catalyst for the degradation of CANs due to its low cost and efficacy. To test our depolymerization procedure, the first attempt made to degrade the linear polymer poly(VL-*co*-$AVL_{0.09}$) with $ZnCl_2$ resulted in a near complete monomer recovery of ∼96%. The dynamic cross-linked network $P_{0.09}$-0.50B, the one with great physical recyclability (Figure 5B), was used to illustrate the chemical depolymerization of a sample that had undergone 5 cycles of physical reprocessing (Figure 5C). Herein, to facilitate the dispersion of catalyst powder in the polymer network, the powder was first dissolved in ethanol and then mixed with shredded polymer network in THF. After removing most organic solvents, the mixture was then subjected to a distillation unit at 180 °C for 4 h. Under the catalysis of $MgCl_2$, the depolymerization product of $P_{0.09}$-0.50B was composed of over 99% oligomers instead of monomers in the recovered product (∼78% according to ^{1}H NMR as illustrated in Figure S32). The degradation products catalyzed by both $ZnCl_2$ and $FeCl_3$ (∼46% and ∼29% monomer recovery, respectively) were mainly oligomers as well (Figure S33). The acid- or alkali-pretreated samples showed even reduced recycling yields via end-group backbiting due to terminal group damage. Through systematic screening of depolymerization catalysts and reaction conditions (Table S9), we established an optimized two-step protocol: deconstruction of polymer network through 1, 2-propanediol-initiated transesterification followed by Sn(Oct)$_2$-catalyzed depolymerization of $P_{0.09}$-0.50B. This approach achieved significantly higher monomer recovery (∼82%) than that without pretreatment (∼58%) (Figure 5D). With recovered monomers, new polymer networks were successfully synthesized after simple purification. The reconstructed polymer network, i.e., $P_{0.09}$-0.50B, exhibited almost identical chemical structure (Figure S34) and comparable mechanical performance (Figures 5B and S28−S30) with pristine sample, achieving circular economy mode.

3. CONCLUSIONS

In summary, this study introduces a novel dual-recycling approach for polymer thermosets, addressing the dilemma between low-energy input yet property downgrading of physical recycling and identical property retention with high-energy cost of chemical recycling. Herein, by copolymerizing δ-VL and α-AVL, functionalized copolymers were successfully synthesized and showcased excellent depolymerizability. Upon reaction with boronic-ester-containing dynamic cross-linkers, the developed CANs demonstrated both excellent mechanical performance and network dynamics. The strategic adjustment of cross-linker proportions balanced the network's crystallinity and cross-linking density, affording a tensile strength of 17.7 MPa and a fracture strain of 1164%. The DMA and rheological studies revealed the terminal relaxation behavior and dynamic bond exchange mechanisms, and such polymer networks retained their structural integrity and functionality over five reprocessing cycles. The dynamic boronic ester bonds enabled efficient reprocessing under mild thermal conditions, while the degradable aliphatic polyester backbone facilitated high-yield monomer recovery through a variety of depolymerization treatment methods. Additionally, the recovered monomers can be effectively repolymerized to produce materials with high-quality properties, supporting a closed-loop recycling process. This innovative dual-recycling strategy aligns with the principles of the circular economy mode, offering a viable pathway for addressing the limitations of traditional thermosets. Looking forward, the dual-recycling CANs present in this work hold considerable potential to inspire future

https://doi.org/10.1021/acs.macromol.5c00904
Macromolecules 2025, 58, 10037−10047

advancements in the development of high-performance recyclable thermosets, paving the way for sustainable polymer design with broader industrial applications and environmental benefits.

4. EXPERIMENTAL SECTION

Experimental details are provided in the Supporting Information.

■ ASSOCIATED CONTENT

Supporting Information

The Supporting Information is available free of charge at https://pubs.acs.org/doi/10.1021/acs.macromol.5c00904.

Synthetic schemes; GPC; NMR; FT-IR; DSC; TGA; cross-linking density test; DMA; creep; rheology; stress relaxation analyses; tensile testing; and recyclability results (PDF)

■ AUTHOR INFORMATION

Corresponding Authors

Zhen Zhang − *South China Advanced Institute for Soft Matter Science and Technology, School of Emergent Soft Matter and Guangdong Provincial Key Laboratory of Functional and Intelligent Hybrid Materials and Devices, Guangdong Basic Research Center of Excellence for Energy and Information Polymer Materials, South China University of Technology, Guangzhou 510640, China*; Email: zhenzhang@scut.edu.cn

Peng-Fei Cao − *State Key Laboratory of Organic−Inorganic Composites, Beijing University of Chemical Technology, Beijing 100029, China; Key Laboratory of Carbon Fiber and Functional Polymers, Ministry of Education, Beijing University of Chemical Technology, Beijing 100029, China*; orcid.org/0000-0003-2391-1838; Email: caopf@buct.edu.cn

Authors

Hongyi Gu − *State Key Laboratory of Organic−Inorganic Composites, Beijing University of Chemical Technology, Beijing 100029, China*

Hao Ju − *State Key Laboratory of Organic−Inorganic Composites, Beijing University of Chemical Technology, Beijing 100029, China*

Kun Chen − *State Key Laboratory of Organic−Inorganic Composites, Beijing University of Chemical Technology, Beijing 100029, China*

Chang Sun − *State Key Laboratory of Organic−Inorganic Composites, Beijing University of Chemical Technology, Beijing 100029, China*

Lin Li − *State Key Laboratory of Organic−Inorganic Composites, Beijing University of Chemical Technology, Beijing 100029, China*

Jiayao Chen − *State Key Laboratory of Organic−Inorganic Composites, Beijing University of Chemical Technology, Beijing 100029, China*

Complete contact information is available at: https://pubs.acs.org/10.1021/acs.macromol.5c00904

Author Contributions

The manuscript was written through contributions of all authors. All authors have given approval to the final version of the manuscript.

Notes

The authors declare no competing financial interest.

■ ACKNOWLEDGMENTS

This research was supported by the National Natural Science Foundation of China (grant nos. 52373275, 22501089, and 52303290, received by P.-F. Cao, Z.Z., and J.C., respectively).

■ REFERENCES

(1) Wu, X.; Hartmann, P.; Berne, D.; De Bruyn, M.; Cuminet, F.; Wang, Z.; Zechner, J. M.; Boese, A. D.; Placet, V.; Caillol, S.; Barta, K. Closed-Loop Recyclability of a Biomass-Derived Epoxy-Amine Thermoset by Methanolysis. *Science* **2024**, *384* (6692), No. eadj9989.

(2) Nicholls, B. T.; Fors, B. P. Closing the Loop on Thermoset Plastic Recycling. *Science* **2024**, *384* (6692), 156−157.

(3) Lei, Z.; Wang, Z.; Jiang, H.; Cahn, J. R.; Chen, H.; Huang, S.; Jin, Y.; Wang, X.; Yu, K.; Zhang, W. Dual-Factor-Controlled Dynamic Precursors Enable On-Demand Thermoset Degradation and Recycling. *Adv. Mater.* **2024**, *36* (45), 2407854.

(4) Robertson, I. D.; Yourdkhani, M.; Centellas, P. J.; Aw, J. E.; Ivanoff, D. G.; Goli, E.; Lloyd, E. M.; Dean, L. M.; Sottos, N. R.; Geubelle, P. H.; Moore, J. S.; White, S. R. Rapid Energy-Efficient Manufacturing of Polymers and Composites via Frontal Polymerization. *Nature* **2018**, *557* (7704), 223−227.

(5) Chen, M.; An, R.; Demoly, F.; Qi, H. J.; Zhou, K. Hybrid 4D Printing of Flexible Multifunctional Composites by Multi Jet Fusion and Direct Ink Writing. *Mater. Sci. Eng. R Rep.* **2025**, *163*, 100890.

(6) Shi, Q.; Wang, T. Mechanochemical Recycling of Highly Cross-Linked Thermosets: Economic-Friendly and Pollution-Free. *Adv. Funct. Mater.* **2024**, *34* (46), 2404848.

(7) Lei, Z.; Chen, H.; Luo, C.; Rong, Y.; Hu, Y.; Jin, Y.; Long, R.; Yu, K.; Zhang, W. Recyclable and Malleable Thermosets Enabled by Activating Dormant Dynamic Linkages. *Nat. Chem.* **2022**, *14* (12), 1399−1404.

(8) Xu, Z.; Liang, Y.; Ma, X.; Chen, S.; Yu, C.; Wang, Y.; Zhang, D.; Miao, M. Recyclable Thermoset Hyperbranched Polymers Containing Reversible Hexahydro-s-Triazine. *Nat. Sustain.* **2020**, *3* (1), 29−34.

(9) Luo, J.; Demchuk, Z.; Zhao, X.; Saito, T.; Tian, M.; Sokolov, A. P.; Cao, P.-F. Elastic Vitrimers: Beyond Thermoplastic and Thermoset Elastomers. *Matter* **2022**, *5* (5), 1391−1422.

(10) Bapat, A. P.; Sumerlin, B. S.; Sutti, A. Bulk Network Polymers with Dynamic B−O Bonds: Healable and Reprocessable Materials. *Mater. Horiz.* **2020**, *7* (3), 694−714.

(11) He, P.; Chen, L.; Shao, L.; Zhang, H.; Lü, F. Municipal Solid Waste (MSW) Landfill: A Source of Microplastics? -Evidence of Microplastics in Landfill Leachate. *Water Res.* **2019**, *159*, 38−45.

(12) Plummer, C. M.; Li, L.; Chen, Y. Ring-Opening Polymerization for the Goal of Chemically Recyclable Polymers. *Macromolecules* **2023**, *56* (3), 731−750.

(13) Shieh, P.; Zhang, W.; Husted, K. E. L.; Kristufek, S. L.; Xiong, B.; Lundberg, D. J.; Lem, J.; Veysset, D.; Sun, Y.; Nelson, K. A.; Plata, D. L.; Johnson, J. A. Cleavable Comonomers Enable Degradable, Recyclable Thermoset Plastics. *Nature* **2020**, *583* (7817), 542−547.

(14) Yang, W.; Ding, H.; Puglia, D.; Kenny, J. M.; Liu, T.; Guo, J.; Wang, Q.; Ou, R.; Xu, P.; Ma, P.; Lemstra, P. J. Bio-renewable Polymers Based on Lignin-derived Phenol Monomers: Synthesis, Applications, and Perspectives. *Sus. Mater.* **2022**, *2* (5), 535−568.

(15) Kamarulzaman, S.; Png, Z. M.; Lim, E. Q.; Lim, I. Z. S.; Li, Z.; Goh, S. S. Covalent Adaptable Networks from Renewable Resources: Crosslinked Polymers for a Sustainable Future. *Chem-US* **2023**, *9* (10), 2771−2816.

(16) Ramakrishna, S.; Jose, R. Principles of Materials Circular Economy. *Matter* **2022**, *5* (12), 4097−4099.

(17) Chen, J.; Li, L.; Luo, J.; Meng, L.; Zhao, X.; Song, S.; Demchuk, Z.; Li, P.; He, Y.; Sokolov, A. P.; Cao, P.-F. Covalent Adaptable Polymer Networks with CO2-Facilitated Recyclability. *Nat. Commun.* **2024**, *15* (1), 6605.

(18) Kloxin, C. J.; Bowman, C. N. Covalent Adaptable Networks: Smart, Reconfigurable and Responsive Network Systems. *Chem. Soc. Rev.* **2013**, *42* (17), 7161−7173.
(19) Podgórski, M.; Fairbanks, B. D.; Kirkpatrick, B. E.; McBride, M.; Martinez, A.; Dobson, A.; Bongiardina, N. J.; Bowman, C. N. Covalent Adaptable Networks: Toward Stimuli-Responsive Dynamic Thermosets through Continuous Development and Improvements in Covalent Adaptable Networks (CANs) (Adv. Mater. 20/2020). *Adv. Mater.* **2020**, *32* (20), 2070158.
(20) Zhang, Z.; Lei, D.; Zhang, C.; Wang, Z.; Jin, Y.; Zhang, W.; Liu, X.; Sun, J. Strong and Tough Supramolecular Covalent Adaptable Networks with Room-Temperature Closed-Loop Recyclability. *Adv. Mater.* **2023**, *35* (7), 2208619.
(21) Luo, J.; Zhao, X.; Ju, H.; Chen, X.; Zhao, S.; Demchuk, Z.; Li, B.; Bocharova, V.; Carrillo, J. Y.; Keum, J. K.; Xu, S.; Sokolov, A. P.; Chen, J.; Cao, P. Highly Recyclable and Tough Elastic Vitrimers from a Defined Polydimethylsiloxane Network. *Angew. Chem., Int. Ed.* **2023**, *62* (47), No. e202310989.
(22) Png, Z. M.; Wang, S.; Yeo, J. C. C.; Raveenkumar, V.; Muiruri, J. K.; Quek, X. C. N.; Yu, X.; Li, K.; Li, Z. Reversible Vitrimisation of Single-Use Plastics and Their Mixtures. *Adv. Funct Materials* **2025**, *35* (1), 2410291.
(23) Wang, J.; You, W.; Chen, L.; Xiao, D.; Xiao, X.; Shan, T.; Liu, Y.; Liu, M.; Li, G.; Yu, W.; Huang, F. Adaptive and Robust Vitrimers Fabricated by Synergy of Traditional and Supramolecular Polymers. *Angew. Chem., Int. Ed.* **2024**, *63* (23), No. e202405761.
(24) Chakma, P.; Konkolewicz, D. Dynamic Covalent Bonds in Polymeric Materials. *Angew. Chem., Int. Ed.* **2019**, *58* (29), 9682−9695.
(25) Fan, X.; Zheng, J.; Yeo, J. C. C.; Wang, S.; Li, K.; Muiruri, J. K.; Hadjichristidis, N.; Li, Z. Dynamic Covalent Bonds Enabled Carbon Fiber Reinforced Polymers Recyclability and Material Circularity. *Angew. Chem., Int. Ed.* **2024**, *63*, No. e202408969.
(26) Su, Z.; Yu, L.; Cui, L.; Zhou, G.; Zhang, X.; Qiu, X.; Chen, C.; Wang, X. Reconstruction of Cellulose Intermolecular Interactions from Hydrogen Bonds to Dynamic Covalent Networks Enables a Thermo-Processable Cellulosic Plastic with Tunable Strength and Toughness. *ACS Nano* **2023**, *17* (21), 21420−21431.
(27) Zhao, J.; Zhang, Z.; Wang, C.; Yan, X. Synergistic Dual Dynamic Bonds in Covalent Adaptable Networks. *CCS Chem.* **2024**, *6* (1), 41−56.
(28) Wang, S.; Feng, H.; Li, B.; Lim, J. Y. C.; Rusli, W.; Zhu, J.; Hadjichristidis, N.; Li, Z. Knoevenagel C = C Metathesis Enabled Glassy Vitrimers with High Rigidity, Toughness, and Malleability. *J. Am. Chem. Soc.* **2024**, *146* (23), 16112−16118.
(29) Kimura, T.; Hayashi, M. One-Shot Transformation of Ordinary Polyesters into Vitrimers: Decomposition-Triggered Cross-Linking and Assistance of Dynamic Covalent Bonds. *J. Mater. Chem. A* **2022**, *10* (34), 17406−17414.
(30) Neidhart, E. K.; Hua, M.; Peng, Z.; Kearney, L. T.; Bhat, V.; Vashahi, F.; Alexanian, E. J.; Sheiko, S. S.; Wang, C.; Helms, B. A.; Leibfarth, F. A. C−H Functionalization of Polyolefins to Access Reprocessable Polyolefin Thermosets. *J. Am. Chem. Soc.* **2023**, *145* (50), 27450−27458.
(31) Parke, S. M.; Lopez, J. C.; Cui, S.; LaPointe, A. M.; Coates, G. W. Polyethylene Incorporating Diels−Alder Comonomers: A "Trojan Horse" Strategy for Chemically Recyclable Polyolefins. *Angew. Chem., Int. Ed.* **2023**, *62* (30), No. e202301927.
(32) Zhao, S.; Liu, Y.; Zhao, H.; Ma, K.; Fu, Y.; Dong, Y.; Li, J.; Pang, C. Catalyst-Free Dynamic Covalent Polyester Networks with Dissociative Transesterification. *Macromolecules* **2024**, *57* (24), 11417−11428.
(33) Li, B.; Ge, S.; Zhao, X.; Chen, Q.; Tian, J.; Hun, D.; Sokolov, A. P.; Saito, T.; Cao, P.-F. Well-Tunable, 3D-Printable, and Fast Autonomous Self-Healing Elastomers. *Supramol. Mater.* **2023**, *2*, 100042.
(34) Feng, H.; Zheng, N.; Peng, W.; Ni, C.; Song, H.; Zhao, Q.; Xie, T. Upcycling of Dynamic Thiourea Thermoset Polymers by Intrinsic Chemical Strengthening. *Nat. Commun.* **2022**, *13* (1), 397.
(35) Liu, X.; Tian, F.; Zhao, X.; Du, R.; Xu, S.; Wang, Y.-Z. Multiple Functional Materials from Crushing Waste Thermosetting Resins. *Mater. Horiz.* **2021**, *8* (1), 234−243.
(36) Kariyawasam, L. S.; Highmoore, J. F.; Yang, Y. Chemically Recyclable Dithioacetal Polymers via Reversible Entropy-Driven Ring-Opening Polymerization. *Angew. Chem., Int. Ed.* **2023**, *62* (26), No. e202303039.
(37) Li, Q.; Ma, S.; Wang, S.; Liu, Y.; Taher, M. A.; Wang, B.; Huang, K.; Xu, X.; Han, Y.; Zhu, J. Green and Facile Preparation of Readily Dual-Recyclable Thermosetting Polymers with Superior Stability Based on Asymmetric Acetal. *Macromolecules* **2020**, *53* (4), 1474−1485.
(38) Lyu, J.; Lee, S.; Bae, H. E.; Jung, H.; Park, Y. I.; Jin, Y.; Jeong, J.; Kim, J. C. Non-Isocyanate Synthesis of Covalent Adaptable Networks Based on Dynamic Hindered Urea Bonds: Sequential Polymerization and Chemical Recycling. *Angew. Chem., Int. Ed.* **2024**, *63*, No. e202411397.
(39) Lyu, J.; Lee, S.; Jung, H.; Park, Y. I.; Ahn, J.; Jin, Y.-J.; Jeong, J.-E.; Kim, J. C. Low-Temperature Chemical Upcycling of Poly-(Ethylene Terephthalate) Waste to Recyclable Polyurethane Thermosets Using Biomass-Derived Materials. *Chem. Eng. J.* **2024**, *501*, 157535.
(40) Qin, B.; Liu, S.; Huang, Z.; Zeng, L.; Xu, J.-F.; Zhang, X. Closed-Loop Chemical Recycling of Cross-Linked Polymeric Materials Based on Reversible Amidation Chemistry. *Nat. Commun.* **2022**, *13* (1), 7595.
(41) Ye, G.; Wang, C.; Zhang, Q.; Song, P.; Wang, H.; Huo, S.; Liu, Z. Bio-Derived Schiff Base Vitrimer with Outstanding Flame Retardancy, Toughness, Antibacterial, Dielectric and Recycling Properties. *Int. J. Biol. Macromol.* **2024**, *278*, 134933.
(42) Li, Z.; Zhao, D.; Shen, Y.; Li, Z. Ring-opening Polymerization of Enantiopure Bicyclic Ether-ester Monomers toward Closed-loop Recyclable and Crystalline Stereoregular Polyesters via Chemical Upcycling of Bioplastic. *Angew. Chem., Int. Ed.* **2023**, *62* (23), No. e202302101.
(43) O'Dea, R. M.; Nandi, M.; Kroll, G.; Arnold, J. R.; Korley, L. T. J.; Epps, T. H. Toward Circular Recycling of Polyurethanes: Depolymerization and Recovery of Isocyanates. *JACS Au* **2024**, *4* (4), 1471−1479.
(44) Zhou, L.; Zhang, Z.; Sangroniz, A.; Shi, C.; Gowda, R. R.; Scoti, M.; Barange, D. K.; Lincoln, C.; Beckham, G. T.; Chen, E. Y.-X. Chain-End Controlled Depolymerization Selectivity in α,α-Disubstituted Propionate PHAs with Dual Closed-Loop Recycling and Record-High Melting Temperature. *J. Am. Chem. Soc.* **2024**, *146* (43), 29895−29904.
(45) Xue, Y.; Zhang, M.; Huo, S.; Ma, Z.; Lynch, M.; Tuten, B. T.; Sun, Z.; Zheng, W.; Zhou, Y.; Song, P. Engineered Functional Segments Enabled Mechanically Robust, Intrinsically Fire-Retardant, Switchable, Degradable PolyureThane Adhesives. *Adv. Funct Materials* **2024**, *34* (49), 2409139.
(46) Wei, P.; Bhat, G. A.; Cipriani, C. E.; Mohammad, H.; Schoonover, K.; Pentzer, E. B.; Darensbourg, D. J. 3D Printed CO_2 -Based Triblock Copolymers and Post-Printing Modification. *Angew. Chem., Int. Ed.* **2022**, *61* (37), No. e202208355.
(47) Xue, Y.; Zhang, T.; Peng, H.; Ma, Z.; Zhang, M.; Lynch, M.; Dinh, T.; Zhou, Z.; Zhou, Y.; Song, P. Fire-Retardant, Anti-Dripping, Biodegradable and Biobased Polyurethane Elastomers Enabled by Hydrogen-Bonding with Cellulose Nanocrystals. *Nano Res.* **2024**, *17* (3), 2186−2194.
(48) Yue, L.; Su, Y.; Li, M.; Yu, L.; Montgomery, S. M.; Sun, X.; Finn, M. G.; Gutekunst, W. R.; Ramprasad, R.; Qi, H. J. One-Pot Synthesis of Depolymerizable δ-Lactone Based Vitrimers. *Adv. Mater.* **2023**, *35* (29), 2300954.
(49) Li, C.; Wang, L.; Yan, Q.; Liu, F.; Shen, Y.; Li, Z. Rapid and Controlled Polymerization of Bio-sourced δ-Caprolactone toward Fully Recyclable Polyesters and Thermoplastic Elastomers. *Angew. Chem., Int. Ed.* **2022**, *61* (16), No. e202201407.
(50) Li, X.; Clarke, R. W.; An, H.; Gowda, R. R.; Jiang, J.; Xu, T.; Chen, E. Y. -X. Dual Recycling of Depolymerization Catalyst and

Biodegradable Polyester That Markedly Outperforms Polyolefins. *Angew. Chem., Int. Ed.* **2023**, *62* (26), No. e202303791.
(51) Schneiderman, D. K.; Hillmyer, M. A. Aliphatic Polyester Block Polymer Design. *Macromolecules* **2016**, *49* (7), 2419−2428.
(52) Ma, K.; An, H.-Y.; Nam, J.; Reilly, L. T.; Zhang, Y.-L.; Chen, E. Y.-X.; Xu, T.-Q. Fully Recyclable and Tough Thermoplastic Elastomers from Simple Bio-Sourced δ-Valerolactones. *Nat. Commun.* **2024**, *15* (1), 7904.
(53) Du, E.; Li, M.; Xu, B.; Zhang, Y.; Li, Z.; Yu, X.; Fan, X. Self-Healing and Adhesive Supersoft Materials Derived from Dynamically Cross-Linked Bottlebrush Polymers for Flexible Sensors. *Macromolecules* **2024**, *57* (2), 672−681.
(54) Fritz-Langhals, E. Unique Superbase TBD (1,5,7-Triazabicyclo[4.4.0]Dec-5-Ene): From Catalytic Activity and One-Pot Synthesis to Broader Application in Industrial Chemistry. *Org. Process Res. Dev.* **2022**, *26* (11), 3015−3023.
(55) Lopalco, A.; Stella, V. J.; Thompson, W. H. Origins, and Formulation Implications, of the pK Difference between Boronic Acids and Their Esters: A Density Functional Theory Study. *Eur. J. Pharm. Sci.* **2018**, *124*, 10−16.
(56) Ricarte, R. G.; Shanbhag, S. A Tutorial Review of Linear Rheology for Polymer Chemists: Basics and Best Practices for Covalent Adaptable Networks. *Polym. Chem.* **2024**, *15* (9), 815−846.
(57) Chen, Q.; Zhao, X.; Li, B.; Sokolov, A. P.; Tian, M.; Advincula, R. C.; Cao, P.-F. Exceptionally Recyclable, Extremely Tough, Vitrimer-like Polydimethylsiloxane Elastomers via Rational Network Design. *Matter* **2023**, *6* (10), 3378−3393.
(58) Amin, D.; Likhtman, A. E.; Wang, Z. Dynamics in Supramolecular Polymer Networks Formed by Associating Telechelic Chains. *Macromolecules* **2016**, *49* (19), 7510−7524.
(59) Liu, Y.; Tang, Z.; Chen, J.; Xiong, J.; Wang, D.; Wang, S.; Wu, S.; Guo, B. Tuning the Mechanical and Dynamic Properties of Imine Bond Crosslinked Elastomeric Vitrimers by Manipulating the Crosslinking Degree. *Polym. Chem.* **2020**, *11* (7), 1348−1355.
(60) Susa, A.; Vogelzang, W.; Teunissen, W.; Molenveld, K.; Maaskant, E.; Post, W. A Direct Comparison of the Thermal Reprocessing Potential of Associative and Dissociative Reversible Bonds in Thermosets. *RSC Appl. Polym.* **2024**, *2* (5), 945−956.
(61) Porath, L.; Soman, B.; Jing, B. B.; Evans, C. M. Vitrimers: Using Dynamic Associative Bonds to Control Viscoelasticity, Assembly, and Functionality in Polymer Networks. *ACS Macro Lett.* **2022**, *11* (4), 475−483.

https://doi.org/10.1021/acs.macromol.5c00904
Macromolecules 2025, 58, 10037−10047